

Water–Hydrocarbon Interfaces: Effect of Hydrocarbon Branching on Interfacial Structure

Janamejaya Chowdhary* and Branka M. Ladanyi

Department of Chemistry, Colorado State University, Fort Collins, Colorado 80523

Received: January 20, 2006; In Final Form: May 12, 2006

Molecular dynamics simulation are performed for the water/hydrocarbon system to study the effect of hydrocarbon branching on interfacial properties. The following two series of hydrocarbons are considered: (1) *n*-pentane, 2-methyl pentane, and 2,2,4-trimethyl pentane (constant chain length) and (2) *n*-octane, 2-methyl heptane, and 2,2,4-trimethyl pentane (constant molecular mass). With a simple algorithm for identification of surface sites and mapping nonsurface sites to these surface sites, intrinsic profiles were constructed with respect to the surface layer. Intrinsic density profiles for water and hydrocarbons with respect to the hydrocarbon and water surface, respectively, resemble density profiles of liquids in the presence of a wall. Order parameters were used to study orientation of molecules with respect to the surface normal and the hydrogen bond network was characterized in terms of the number of hydrogen bonds per water molecule and percentage of hydrogen bonded molecules in the first coordination shell. The corresponding intrinsic profiles were obtained. The O–H bond for surface water was found to have two preferential orientations, pointing toward the hydrocarbon phase and parallel to the interface. Hydrocarbon molecules in series 1 orient along the interface with the more branched molecule better aligned. For molecules in series 2, the larger molecular length reduces the alignment of molecules along the interface.

I. Introduction

Liquid–liquid interfaces are ubiquitous in nature and many phenomena of scientific and technological importance, such as electron or ion transfer¹ and surfactant assembly² to form micelles or reverse micelles, occur at these interfaces. With water being the prominent liquid on Earth, it is not surprising to find it as a component of a large number of liquid/liquid interfaces. A simple liquid/liquid interface involving water is the water/hydrocarbon interface which not only is relevant for oil extraction³ but also serves as a model for understanding the hydrophobic effect.^{4–6} A molecular level understanding of such surfaces is crucial for insight into interfacial phenomenon and remains an active area of research.⁷

For hydrocarbon systems, branching of the molecule can lead to materials with improved (over linear hydrocarbons) industrially significant rheological properties, for example, lubrication, besides playing a role in the reverse micelle forming ability of surfactants. We are therefore interested in studying the effect of hydrocarbon branching on water/hydrocarbon interfaces.

An interface can be characterized in terms of the density profile, orientation of molecules at and away from the interface, and intermolecular correlations at the interface.⁸ Most theoretical insight on interfaces has originated in attempts to understand the liquid/vapor and liquid/solid interfaces although their conclusions can be easily extended to liquid/liquid interfaces. These insights fall into two distinct categories. The first is the mean field approach pioneered by van der Waals⁹ with refinements by Cahn and Hillard,¹⁰ and Widom and co-workers.¹¹ This approach assumes the existence of a continuous density profile referred to as the “intrinsic” density profile. The intrinsic profile typically has a hyperbolic tangent functional form for a liquid/vapor interface. The two coexisting phases

are separated by a transition region with a width proportional to the bulk correlation length and independent of system size or external force. Approaching the critical point of the system leads to a diverging correlation length and consequently a diffuse interface. The second approach, that of the capillary wave model (CWM),¹² assumes a step function intrinsic density profile that is broadened by thermally activated long wavelength capillary waves. The density profile so obtained has the form of an error function with a width that is system size dependent. The distribution of surface sites has a Gaussian functional form.

While the first approach ignores the degrees of freedom associated with the interface, the second focuses on the interface only. The complete picture would likely give appropriate weight to both. Weeks¹³ reconciled these two approaches by arguing that they apply at different length scales. The intrinsic profile then refers to structure of the interface with an area of cross section of the order of bulk correlation length squared for the liquid/vapor interface. Integrating out the small scale degrees of freedom from the total Hamiltonian of the system then leads to the capillary wave Hamiltonian. Of course, the length scale at which CWM becomes appropriate is hard to define due to continuity of scales at the interface. The usually accepted view of interfacial structure is that of an intrinsic profile attached to the surface which in turn is broadened by capillary waves. Following Percus,¹⁴ for a distribution of surface positions, $P(\xi)$, described by the CWM, and an intrinsic profile, $\rho_i(z)$, with respect to this interface, the density profile can be expressed in the “convolution approximation” (CA) as

$$\rho(z) = \int_{-\infty}^{\infty} d\xi P(\xi) \rho_i(z - \xi) \quad (1)$$

where it is assumed that surface positions are uncorrelated with the intrinsic density profile. The total interfacial width is the sum of the CWM contribution to surface broadening and the width of the intrinsic profile.

* To whom correspondence should be addressed. E-mail: janamej@lamar.colostate.edu; Branka.Ladanyi@colostate.edu.

Experimental characterization of the water/hydrocarbon interfacial structure has been limited since interfaces are by nature buried and deviations from bulk are typically limited to a small spatial region in the vicinity of the interface. Electronic or atomic density profiles normal to the interface are typically obtained using X-ray or neutron reflectivity experiments.^{15–18} The width of an interface can be extracted from the wave-vector transfer dependence of reflectivity, and intrinsic density profiles can in principle be obtained by deconvolution of the experimental density profiles. Orientation of probe molecules at an interface can be probed using sum-frequency generation.¹⁹ At aqueous interfaces, the O–H stretching modes of surface water can be studied using vibrational sum-frequency spectroscopy and interpreted in terms of the number of hydrogen bonded water molecules thereby providing insight into the orientation of water at interfaces. For water/hydrocarbon interfaces involving *n*-hexane, *n*-heptane, and *n*-octane, the vibrational sum-frequency spectra of water were found to be qualitatively similar and dominated by water molecules with fewer than four hydrogen bonds.²⁰

Computer simulations can provide more detailed information than a particular experiment for interfacial structure and dynamics. There have been molecular dynamics simulations of the water/hydrocarbon system for the following hydrocarbons: *n*-pentane,²¹ *n*-hexane,^{21–25} *n*-heptane,²¹ *n*-octane,^{21,26–28} *n*-nonane,^{21,29} *n*-decane,^{21,23,30} *n*-hexadecane,²³ and isooctane.³¹ These studies have mostly focused on density profiles, orientation of molecules, surface tension, solvation thermodynamics or dynamics at the interface in addition to testing the predictions of the capillary wave model. Direct comparison of the simulation results for the same water/hydrocarbon system in different studies, for example, water/*n*-octane,^{21,26,27} is not straightforward due to differences in simulation methodology, conditions, and force fields. Simulation of the vibrational sum-frequency spectrum for the water/*n*-hexane system gave results in good agreement with experiments.²⁰

In view of the CA (eq 1), experimental and simulated density profiles can be interpreted as broadened intrinsic profiles. Any structure present in the intrinsic profile is likely to be lost or reduced due to capillary waves acting on the interface. Filtering out the capillary wave contribution to surface fluctuations allows for a better understanding of interfacial structure in terms of intrinsic profiles. The effect of hydrocarbon branching on water/hydrocarbon interfaces will therefore be studied in terms of the intrinsic structure in this work.

This paper is organized as follows. Section II contains the methodology, conditions, and force fields used for the simulation. A simple procedure for identifying surface sites and constructing intrinsic profiles with respect to the surface is also presented. In section III, various intrinsic density profiles with respect to water and hydrocarbon surfaces as well as the usual density profiles are constructed. The convolution approximation relating the intrinsic and density profiles is tested. In section IV, orientation of molecules is studied in terms of orientation and intrinsic orientation profiles. Finally, in section V, hydrogen bonding of water molecules near and away from the interface is analyzed. Our conclusions on the effect of hydrocarbon branching on the interface are summarized in section VI at the end.

II. Simulation Details

A. Molecular Dynamics Simulation. Molecular dynamics simulations are carried out with codes developed in our group. All molecular bond lengths and angles are treated as fixed and

TABLE 1: Details of the Simulation Setup^a

hydrocarbon	N_h	ρ	L	$\langle L_z \rangle$
<i>n</i> -pentane (P)	91	0.625	25.98	78.44
2-methyl pentane (2MP)	79	0.650	25.98	76.94
2,2,4-trimethyl pentane (TMP)	64	0.692	25.98	78.51
2-methyl heptane (2MH)	64	0.698	25.98	76.71
<i>n</i> -octane (O)	64	0.702	25.98	76.76

^a The number, N_w , of water molecules is fixed at 586, number of hydrocarbon molecules (N_h), bulk densities in g/cm³ for the hydrocarbon (ρ), lateral dimension of the interface, L , in angstroms, and length of the simulation box, L_z , in angstroms.

constrained to their equilibrium values using RATTLE.³² The three site SPC/E model³³ is adopted for water whereas a united atom representation is selected for the hydrocarbon molecules with site–site interactions and torsions described by the OPLS force field³⁴ except for branched hydrocarbons where the torsional parameters are supplemented.³⁵ The usual Lorentz–Berthelot combination rules were used to describe Lennard–Jones interactions between dissimilar sites.³⁶

Coulombic interactions were handled with Wolf’s method³⁷ which treats them as a spherically truncated damped pairwise potential. This method has been successfully applied to bulk studies of molten salts, aluminosilicates, and water^{37–39} as well as in a study of ferroelectric properties of PbTiO₃ thin films.⁴⁰ For water, structure, dynamics, and electrostatics have been found to be comparable with the standard Ewald summation method albeit with lesser computational requirement. A truncation radius of 9 Å and damping constant of 0.2 Å^{−1}, analogous to the Ewald method, was used in the implementation of Wolf’s method throughout the simulation. For comparison, the simulation was repeated for the water/pentane system using the Ewald summation, and no significant differences in the energies and intrinsic profiles (section III A) with respect to Wolf’s method were found.

Pressure was calculated based on the virial.³⁶ The kinetic definition of temperature was adopted instead of the configurational temperature.⁴¹ The temperature and pressure were maintained constant at 298.15 K and 1 atm using Berendsen’s thermostat and barostat⁴² with a coupling constant of 20 ps and an MD time step of 2 fs. The effect of varying the coupling constants in Berendsen’s thermostat on the energies and interfacial structure was found to be negligible. While the Berendsen thermostat does not sample the ensemble correctly,⁴³ it does not appear to have a significant effect on interfacial structure.

Simulation of the water/hydrocarbon interface was carried out in two steps. First, constant temperature configurations were generated for $N_w = 586$ water molecules in a cubic box with box length selected to give a density of 1.0 g/cm³. The hydrocarbon molecules were simulated in a cuboidal box with an area of cross-section identical to the water box but with a length selected to give the experimental densities. The number of molecules, density, and average length of the sides of the simulation box are summarized in Table 1. Next, an equilibrium water configuration is sandwiched between two identical copies of the equilibrium hydrocarbon configuration along the z -direction with the (x, y) plane representing the shared face of the water and hydrocarbon boxes. Unfavorable interactions were minimized by performing MD simulations with a time step that increased at a constant rate from 0.001 to 2 fs over 25 000 time steps. After this, the system is allowed to equilibrate at constant temperature and pressure for 250 ps and configurations were saved every 20 fs from an additional 1 ns simulation for a total of 50 000 configurations.

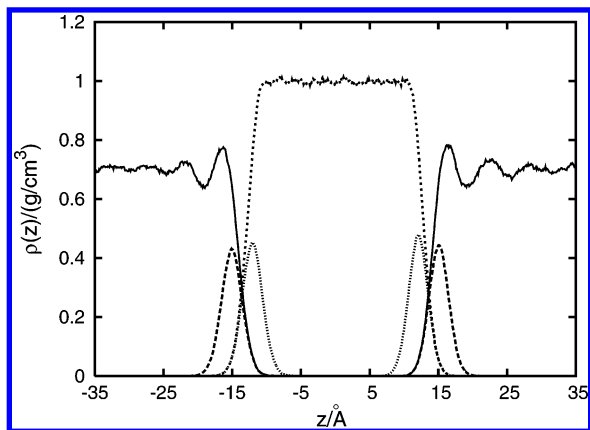


Figure 1. Density profiles for the water (small dashes) and 2,2,4-trimethyl pentane (solid line) interface. Also shown in the figure are contributions of hydrocarbon (large dashes) and water (dotted line) surface molecules to the density profile for the four surfaces.

Two series of liquid/liquid interfaces are studied differing in the hydrocarbon component which is changed to study the effect of branching of the hydrocarbon on interfacial properties. In series 1, the chain length is kept constant for pentane (P), 2-methyl pentane (2MP), and 2,2,4-trimethyl pentane (TMP) and for series 2, the molecular mass is held fixed for octane (O), 2-methyl heptane (2MH), and 2,2,4-trimethyl pentane (TMP). The simulation procedure is identical for each water/hydrocarbon system. The density profiles for the water/2,2,4-trimethyl pentane system is shown in Figure 1 to illustrate the system setup.

B. Surface Layer Identification and Intrinsic Profile Construction. The first step in constructing an intrinsic profile is identification of the intrinsic surface with respect to which the profiles are to be constructed. Traditionally, an intrinsic surface is identified with the Gibbs dividing surface.⁸ One could then follow Weeks¹³ suggestion, partition the surface into grids with an edge equal to the correlation length of the system, identify the position of the local Gibbs surface for each grid, and construct a smooth surface passing through the position of the local Gibbs surface for each grid. The intrinsic surface so obtained does not necessarily pass through the atomic sites that represent the instantaneous interfacial configuration, and analysis of fluctuations of this surface indicates a failure in separation of surface and bulk degrees of freedom.^{44–46} Alternative definitions for a surface that successfully separates surface and bulk degrees of freedom are therefore needed.

Since atomic level information is available, it would be useful to identify a set of atoms/sites and define a surface based on them. For each component of the liquid/liquid interface, partitioning the interface into grids analogous to Weeks local Gibbs surface construction and identifying the local surface position with the atom/site with maximal penetration into the other liquid phase for that grid is one procedure for identification of the set of surface sites.⁴⁷ Another possibility, used for water/phospholipid bilayers, is to identify the phosphorus atom of the phospholipid with the set of surface sites.⁴⁸ Alternatively, the set of surface sites can be identified based on their local coordination.^{44,45}

For the simulation setup used here, there are two water/hydrocarbon interfaces for each configuration. We therefore need to identify four intrinsic surfaces, two each for water (W) and the hydrocarbon (H). The surface layer for a given component of the interface by definition must include sites of that liquid which are closest to the second liquid component. We represent each water molecule by its oxygen atom and the

hydrocarbon molecule with its united atom sites. For each site i of molecular species A ($= \{H, W\}$), the site j of species B ($= \{W, H\}$), with the smallest Cartesian distance from i is labeled as a B surface site. Surface sites of A can be identified in a similar manner. For each hydrocarbon site i , sites on the same molecule closer to the water surface than i , if present, are added to the list of hydrocarbon surface sites. By projecting all water molecules i within 3.5 Å of each water surface molecule j onto the (x, z) and (y, z) plane, if i and j overlap, molecule i is added to the list of surface water molecules.

Density profiles or equivalently the distribution of surface sites can be easily constructed based on the set of surface positions and are shown in Figure 1 for the two water and hydrocarbon surface layers along with the density profile for each component. The surface density profile represents a small spatial region in the vicinity of the interface, makes a small contribution (<0.4 g/cm³) to the overall density profile, and does not include sites in the bulk phase. These four distributions are located symmetrically about the center of the water slab which has been selected as the origin of coordinates for the simulation. The corresponding distribution of surface sites has a Gaussian form consistent with CWM predictions and will be analyzed elsewhere.⁴⁹

With the set of surface positions available, a 2-D Fourier series representative of a continuous surface passing through all surface sites, subject to minimal surface area requirement, can be obtained and intrinsic profiles constructed based on it.^{44–46} This procedure is computationally expensive due to the fitting necessary for obtaining the Fourier coefficients. We therefore adopt an alternative procedure similar to the one used by Pandit et al.⁴⁸ for a phospholipid–water interface. Let $\xi(\mathbf{r}_i)$ be the z -coordinate of a surface site i at a point \mathbf{r}_i in the (x, y) plane. Project all surface sites onto the (x, y) plane located at $z_0 = \langle \xi(\mathbf{r}_i) \rangle$ and perform a Voronoi tessellation of the (x, y) plane at $z = z_0$. Project each nonsurface site j onto the $z = z_0$ plane, identify the surface site i whose Voronoi simplex it falls into, and assign $i \leftarrow j$. The separation between the two sites, an approximation to the distance from the surface, along the z -direction is $z_j - \xi(\mathbf{r}_{i \leftarrow j})$. Each molecular site can now be mapped to a surface site and intrinsic profiles constructed as a function of distance from this surface.

Assignment of sites that form one surface to sites on the other proximal surface forming the interface can be tricky. For each water molecule that penetrates the hydrocarbon phase, the oxygen atom can be assigned to any of the nearest hydrocarbon surface sites forming the cavity. A unique hydrocarbon site is then selected depending on proximity and subject to the hydrocarbon site not falling inside the HOH triangle in projections of the water molecule onto the (x, z) and (y, z) planes. The same two conditions must be satisfied for assignment of surface hydrocarbon sites to oxygen surface sites. In some cases, a unique assignment is not possible and might result in assignment of $\sim 1\%$ of surface sites to the vicinity of the reference surface layer. This is not expected to make a significant contribution to the resulting intrinsic profiles.

For some property \mathbf{X}_j that depends on nonsurface site j 's position, the intrinsic profile $\mathbf{X}_i(z)$ can be defined as

$$\mathbf{X}_i(z) = \left\langle \sum_{j=1} \mathbf{X}_j \delta[z - \{z_j - \xi(\mathbf{r}_{i \leftarrow j})\}] \right\rangle \quad (2)$$

and the usual average profile, $\mathbf{X}(z)$, independent of the intrinsic surface is

$$\mathbf{X}(z) = \left\langle \sum_{j=1} \mathbf{X}_j \delta[z - z_j] \right\rangle \quad (3)$$

These could possibly be related via the “convolution approximation”, for example, as is done for densities in eq 1.

III. Density Profiles

A fundamental characterization of an interface is in terms of its density profile which can be easily constructed in simulations and measured experimentally. For a system composed of molecules each having a total mass M and N sites (atomic or united atom), this corresponds to selecting $\mathbf{X}_j = (M/N)$ for each site j or $\mathbf{X}_j = M$ for molecule j when using the center of mass positions in eq 3. The corresponding intrinsic density profiles can be constructed as defined in eq 2.

For the water/hydrocarbon system, it is possible to construct surface pinned intrinsic profiles with respect to either the water or hydrocarbon surface. There are therefore a total of four possible intrinsic profiles: $\rho_1^{\text{H-W}}(z)$, $\rho_1^{\text{W-W}}(z)$, $\rho_1^{\text{H-H}}(z)$, and $\rho_1^{\text{W-H}}(z)$ where we use the notation that the subscript A–B refers to the intrinsic profile of A with respect to the surface of B.

The intrinsic density profiles are constructed and analyzed in section III A while the usual density profiles are presented in section III B. They are analyzed and the effect of hydrocarbon branching discussed. Finally, at the end, the validity of the convolution approximation is tested and the choice of different functional forms to model intrinsic density profiles addressed.

A. Intrinsic Density Profile. 1. Water. Hydration structure in the vicinity of an extended hydrocarbon surface is best quantified in terms of the intrinsic density profile of water, represented by the position of the oxygen atom, with respect to the hydrocarbon surface, $\rho_1^{\text{W-H}}(z)$. The effect of hydrocarbon branching on this profile is small for both series 1 and 2 so we present data only for series 1 in Figure 2a.

Implicit in the definition of this intrinsic profile is the presence of a hydrocarbon site at $z = 0$. A simple reference system that resembles this is water in the vicinity of a planar structureless hydrophobic wall at $z = 0$. The overall shape of $\rho_1^{\text{W-H}}(z)$ is not surprisingly similar to the density profile of water for this reference system.⁵⁰ However, unlike the planar reference system, the hydrocarbon surface is structured and rough allowing water molecules to penetrate the hydrocarbon phase. This leads to a finite but small density of water molecules within ~ 2 Å of the surface. There is a slight shoulder at $z \sim 1$ Å which is perhaps due to these penetrant molecules.

The asymptotic density of water away from the hydrocarbon surface is approximately 0.997 g/cm^3 which is the density of bulk SPC/E water at STP.³³ This validates the procedure adopted for construction of $\rho_1^{\text{W-H}}(z)$. Deviation from bulk density is confined to within ~ 10 Å from the surface in Figure 2a with two prominent peaks at 3.6 and 7.2 Å in agreement with previous studies.⁴⁷

The position of this first peak corresponds to water molecules that are nearest neighbors to hydrocarbon surface sites. The hydrocarbon surface area is larger than an equivalent planar system due to surface roughness brought about by thermal fluctuations. More molecules can be accommodated at this surface contributing to this enhanced density. Of course, due to the hydrogen bonded network forming ability of water, the first peak indicates a preferred arrangement at the surface as well. The height and shape of the first peak depend on the number of molecules forming the water surface and their arrangement at the surface. The number of surface water

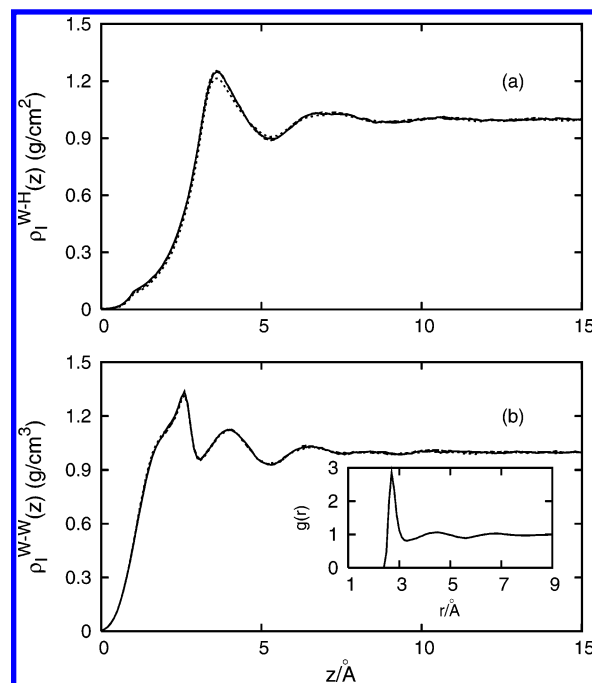


Figure 2. Intrinsic number density profiles for water (a) with respect to the hydrocarbon surface layer, $\rho_1^{\text{W-H}}(z)$, and (b) with respect to the water surface layer, $\rho_1^{\text{W-W}}(z)$. Results are shown for hydrocarbon series 1: P (solid line), 2MP (large dashes), and TMP (small dashes). Also inset in (b) is the bulk water O–O pair distribution function.

molecules per unit area is 0.06 ± 0.002 , 0.06 ± 0.002 , and $0.06 \pm 0.003 \text{ Å}^{-2}$ for the P, 2MP, and TMP interfaces. Since these numbers are comparable, the heights should be similar and that is indeed the case.

The region between the hydrocarbon surface and first layer of water molecules has a small density of sites and is sufficiently large, ~ 3.6 Å, for the system to accommodate voids. The free energy cost of cavity formation necessary to solvate small molecules with size of the order of methane is therefore reduced at the interface. A decrease in density in the vicinity of the hydrocarbon surface layer is akin to the “drying” scenario at extended hydrocarbon surfaces that has been invoked in the context of the hydrophobic solvation.⁵ The second peak at ~ 6.9 Å is wider than the first. Since the O–O distance for the hydrogen bonded molecule is ~ 3.5 Å, the position of this peak corresponds to the second layer of hydrogen bonded water molecules adjacent to the surface water layer.

Since $\rho_1^{\text{W-H}}(z)$ represents the density of water with respect to a reference surface formed by hydrocarbon sites, it is tempting to interpret it in terms of the local hydration structure for surface hydrocarbon molecules. For a water/ n -C₁₈ interface with hydrocarbon molecules tethered to a surface, Ashbaugh et al.⁵¹ related the density profile of water to the hydration structure about each hydrocarbon molecule. Since the hydrocarbon molecules were tethered in their study, capillary wave contributions to interface broadening were minimal and the density profile of water was equivalent to $\rho_1^{\text{W-H}}(z)$. However, unlike in their system, the hydrocarbon molecules here are free to rotate and it is not clear how their analysis can be applied here. At best, one could think of this intrinsic density profile as arising from the local hydration structure of hydrocarbon molecules with different orientations in space with respect to the water layer.

An alternate probe of water structure beyond the surface water layer is the intrinsic density profile of water with respect to the water surface layer. This intrinsic profile, $\rho_1^{\text{W-W}}(z)$, is con-

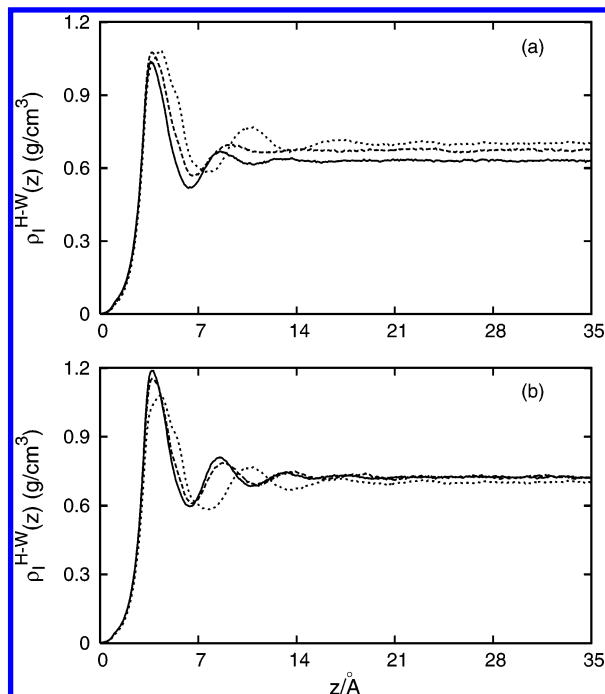


Figure 3. Intrinsic number density profiles for the hydrocarbon with respect to the water surface, $\rho_l^{H-W}(z)$ for (a) series 1: P (solid line), 2MP (large dashes), and TMP (small dashes); (b) series 2: O (solid line), 2MH (large dashes), and TMP (small dashes).

structured and shown in Figure 2b. Since each nonsurface oxygen site is mapped to a surface oxygen site, comparison with the oxygen–oxygen pair distribution function would appear natural. In fact, $\rho_l^{W-W}(z)$ resembles the bulk oxygen–oxygen pair distribution for $z \geq 2.6$ Å with the position of the first three peaks at ~ 2.6 , 4.2 , and 6.8 Å comparable with those for the oxygen–oxygen pair distribution at ~ 2.7 , 4.5 , and 6.8 Å (Figure 2b Inset). This intrinsic profile is of course distinct from a pair distribution function although by analogy with Ashbaugh et al.⁵¹ it could be thought of as representing hydration structure with respect to surface water molecules.

Despite similarities with the oxygen–oxygen pair distribution, a significant difference is the appearance of a shoulder in the first peak at $z \sim 2.6$ Å. This feature is absent from the bulk oxygen–oxygen pair distribution function and implies a modification of the water network perhaps indicating two preferred orientations and two preferred positions. Fluctuations in the position of the surface layer if sufficiently large would broaden this shoulder leading to a single peak in $\rho_l^{W-H}(z)$.

Dependence on the hydrocarbon component of the interface is even weaker for $\rho_l^{W-W}(z)$ than that for $\rho_l^{W-H}(z)$ due to distance from the hydrocarbon phase. In light of the insignificant effect of hydrocarbon branching on the second peak in $\rho_l^{W-H}(z)$, it is not surprising to find a similar structure of water adjacent to the surface water layer for all hydrocarbons in series 1. While not shown in the figure, hydrocarbons in series 2 have a similar weak effect on the water surface.

2. Hydrocarbon. So far, we have discussed the structure of water with respect to the hydrocarbon surface. The intrinsic profile for hydrocarbon molecules with respect to the water surface, $\rho_l^{H-W}(z)$, provides a complementary view of the interface and is presented in Figure 3. These intrinsic profiles are more structured and exhibit a stronger dependence on hydrocarbon branching than for water intrinsic profiles. Furthermore, they resemble the density profile of hydrocarbon molecules in the presence of a soft wall.⁵²

TABLE 2: Analysis of Surface Sites Is Presented for Each Water/Hydrocarbon Interface^a

hydrocarbon	p_a	p_{0-Me}	N_s	l_{Me-Me}
P	32.24	52.48	44	4.6
2MP	41.41	40.52	45	4.5
TMP	48.38	24.98	45	4.4
2MH	33.36	53.32	50	6.4
O	22.97	67.45	51	7.5

^a Percentage of surface molecules contributing at least one methyl site from each terminus, p_a , percentage of non-methyl surface sites, p_{0-Me} , number of surface sites, N_s , and average end-to-end cartesian distance, l_{Me-Me} in angstroms.

A prominent feature in $\rho_l^{H-W}(z)$ is the presence of a sharp peak in the vicinity of the water surface. This sharp peak is indicative of enhanced local density which could arise due to stacking of hydrocarbon molecules along the plane of the interface. Previous simulations of water/linear hydrocarbon interfaces²¹ seem to support this inference, and visual inspection for each interfacial system studied here seems to corroborate this scenario.

It would be useful to quantify the extent of stacking to gain insight into the structure of the first peak. Molecules that stack at the surface must orient in the plane of the surface locally in addition to possibly being neighbors to similarly oriented molecules. Due to their orientation along the surface, they are likely to contribute methyl sites to the surface from either terminal of the molecule. We therefore estimate the percentage of surface molecules, p_a , that contribute at least one methyl site to the surface from both terminals of the molecule. The average value of p_a averaged over the two hydrocarbon surfaces is presented in Table 2.

While not directly observable in the intrinsic density profile, p_a is nonetheless a useful quantity. For series 1, p_a increases with branching from P to TMP suggesting an increase in the number of molecules orientated along the surface. The average distance between the terminal methyl groups at the two terminals of the molecule, l_{Me-Me} , is essentially constant for this series. An increase in p_a is therefore expected to be primarily a consequence of an increase in branching. The more branched structure oriented along the surface would contribute more methyl sites, and this is indeed the case as shown by the decrease in percentage of nonmethyl sites, p_{0-Me} , at the surface from TMP to P.

On the other hand for series 2, the decrease in p_a from TMP to O, Figure 3b, is associated with an increase in l_{Me-Me} by a factor of ~ 1.7 . For a constant cross-sectional area, more molecules can fit in the plane of the surface if they are short. The length of the molecule therefore appears to be the dominant factor, and p_a decreases from TMP to O. For 2MH and O, the number of surface sites is comparable but the length of the molecule increases. The associated decrease in percent of aligned molecules is again consistent with expectation based on molecular length alone.

Another consequence of the decrease in the number of molecules oriented in the plane of the surface is the increase in available free space at the surface for other molecules. Consequently, the number of surface sites, N_s , increases from TMP to O in Table 2. Associated with this increase in N_s is an increase in peak height from TMP to O. For series 1, the number of surface sites is comparable and so are the peak heights.

Width and position of the first peak are also affected by branching. The more branched molecule has a larger girth and is better aligned at the surface. Consequently, the first peak should broaden with branching while the position of the center of this peak should shift away from the water surface. This in

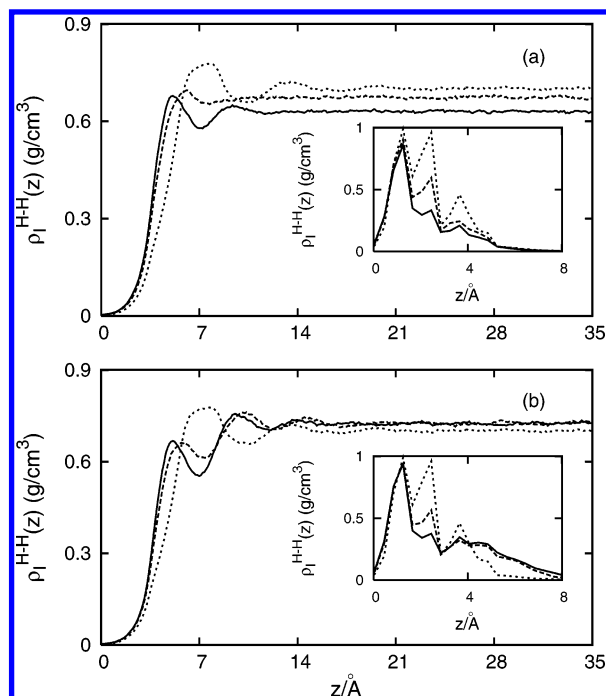


Figure 4. Intrinsic number density profiles for the hydrocarbon with respect to the hydrocarbon surface, $\rho_I^{H-H}(z)$ for (a) series 1: P (solid line), 2MP (large dashes), and TMP (small dashes); (b) series 2: O (solid line), 2MH (large dashes), and TMP (small dashes) where hydrocarbon molecules that contribute sites to the surface are ignored. The shown inset is the contribution from molecules that contribute sites to the hydrocarbon surface. The same line types are used for different hydrocarbons in the inset as in the main plot.

fact is the trend observed, for example, in Figure 3b where the position of the first peak shifts from ~ 4 Å for O to 4.2 and 4.5 Å for 2MH and TMP, respectively.

Branching has a more pronounced effect on the second peak. The position of this peak shifts from 9 to 9.3 and 10.9 Å from O to TMP in series 2. Since chain lengths decrease with branching for series 2, this second peak cannot solely be due to molecules oriented perpendicular to the surface. A better probe of the underlying structure is the intrinsic density profile for hydrocarbon molecules with respect to the hydrocarbon surface. Since $\rho_I^{H-H}(z)$ includes molecules that contribute sites to the surface, the small number of surface molecules would lead to poor statistics and averaging. We therefore calculate contributions from the nonsurface and surface molecules separately.

Intrinsic density profiles for nonsurface molecules with respect to the hydrocarbon surface are presented in Figure 4 for hydrocarbon series 1 and 2. The shown inset in Figure 4 is the contribution from surface molecules only. For surface hydrocarbon molecules, while noisy, the presence of peaks close to the hydrocarbon surface is an indication of preferred orientation of molecules at the surface. In light of the data on p_a , the presence of peaks is to be expected. Series 2 consists of longer molecules, and the larger spatial extent of this intrinsic profile for surface molecules would suggest a finite population of molecules aligned perpendicular to the surface.

The intrinsic density profile, $\rho_I^{H-H}(z)$, for surface molecules indicates most sites are concentrated within ~ 5 Å from the surface layer. There are a few nonsurface molecules in this region as reflected in the very small but finite density due to them. The presence of a peak in $\rho_I^{H-H}(z)$ for nonsurface molecules is indicative of preferential arrangement with respect to the surface molecules. For series 1, the peaks are structureless

and are located at distances of 5.1, 6.11, and 7.6 Å from the surface for P, 2MP, and TMP. Their position should depend on the orientation of surface molecules as well as preferred orientations of nonsurface molecules with respect to them which is hard to determine from the intrinsic density profile. The increase in height with branching is due to the addition of methyl sites, but their magnitudes are smaller as compared with the peak height based on surface molecules suggesting a more diffuse and bulklike ordering than the surface layer.

Series 2 on the other hand shows a peculiar behavior in its first peak. The maximum density corresponding to this peak is smaller than the bulk value, unlike in series 1, where it is always larger, but indicative of a preferred separation from the surface. Surface molecules in this hydrocarbon series do not orient in the plane of the surface and are expected to adopt a range of orientations. Consequently, there is a decrease in the number of nonsurface molecules in the vicinity of the surface layer leading to sub-bulk density for the first peak.

The second peak in $\rho_I^{H-H}(z)$ shifts away from the hydrocarbon surface for the more branched molecule. For series 1, density reaches asymptotic bulklike values beyond the second peak except for TMP. There is some structure for TMP that lasts up to at least 22 Å from the hydrocarbon surface suggesting the size of the simulation box along the z -axis should be at least twice (two water–hydrocarbon interfaces) this value to accommodate these long-range fluctuations. For series 2, besides TMP, O, and 2MH exhibit at least two more peaks beyond the second before reaching bulklike unstructured values. The longer length of these molecules is the likely reason for this enhanced ordering as compared with P and 2MP.

B. Density Profile. With interfacial positions and intrinsic profiles available, the density profile for each component of the water/hydrocarbon interface can be interpreted in terms of the convolution approximation. Peaks in the intrinsic profiles are expected to broaden or vanish in the corresponding density profiles due to surface fluctuations. In this section, we present the density profiles for each component of the interface.

In our simulation setup, there are two equivalent interfaces and we present density profiles for the system for $z > 0$. Density profiles for water at interfaces formed by hydrocarbons in series 1 are shown in Figure 5a. These water profiles are identical for all hydrocarbons. The structure observed in $\rho_I^{W-H}(z)$ is completely lost upon convoluting it with the distribution of hydrocarbon surface positions, and the resultant structureless density profile for water has an error function form. Such density profiles have been observed in previously reported studies of the water/hydrocarbon interface.^{21,27} However, there are simulation studies, for example, for water–octane interfaces²⁶ where the peaks in the intrinsic profile do not wash out for water. The origin of this difference is unclear.

Density profiles for the hydrocarbon component of the interface have more structure than for water. The height of the first peak for series 1 increases while the peak position shifts to large z values in Figure 5b. This is analogous to the structure in $\rho_I^{H-W}(z)$ broadened due to fluctuations of the water surface although not completely washed out as in the case of water, a feature shared with previous simulation studies.^{21,26,27} A similar trend can be seen for hydrocarbon in series 2 (Figure 5). Branching appears to broaden the first and second peaks in addition to shifting the peak to larger z for hydrocarbons with the same mass but different extent of branching.

Density profiles obtained from simulations are typically modeled in terms of the CWM where the intrinsic density profile is assumed to have the step function form, $\rho_I(z) = \rho_0\Theta(z - z_0)$

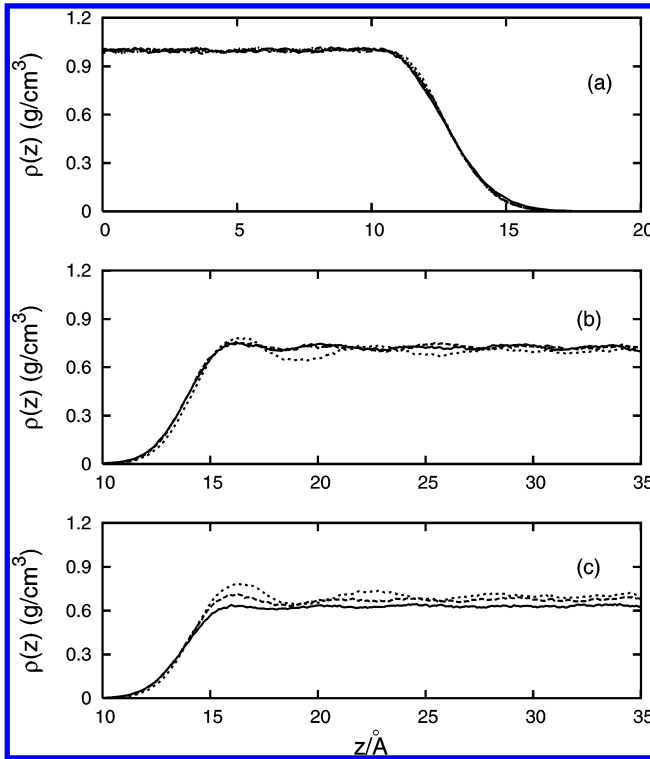


Figure 5. Density profiles $\rho(z)$ for (a) water: the different systems are P (solid line), 2MP (large dashes), and TMP (small dashes); (b) series 2: P (solid line), 2MP (large dashes), and TMP (small dashes); and (c) series 1: O (solid line), 2MH (large dashes), and TMP (short dashes).

where ρ_0 is the bulk density and Θ is the Heaviside function. This intrinsic profile is broadened due to the Gaussian distribution of surface sites with mean ξ_0 and variance σ^2 . Defining $z_1 = z_0 + \xi_0$, the resultant density profile, $\rho(z)$, has the form

$$\rho(z) = \frac{\rho_0}{2} \left\{ 1 + \operatorname{erf} \left[\frac{z - z_1}{\sqrt{2}\sigma} \right] \right\} \quad (4)$$

The advantage of this error function form is the ease of fitting the density profiles obtained from simulation or experiments and extracting a capillary wave broadened width for the surface. Intrinsic density profiles revealed by our simulations are clearly not described, except asymptotically, by an error function. While one may fit the density profile to an error function approximately, the interfacial width so obtained might not represent the actual value. As a simple approximation, borrowing from liquid state theories for the pair distribution function, the intrinsic profile could be represented by an exponentially damped sinusoidal. An alternate simpler approximation for the intrinsic profile has the form

$$\rho_1(z) = \left[A + B \exp \left(-\frac{z - z_0}{\lambda} \right) \right] \Theta(z - z_0) \quad (5)$$

where A , B , λ , and z_0 are parameters to be determined from a fit to the intrinsic profile with respect to the same surface. If we consider the intrinsic profile with respect to the water surface, the parameter A is by definition the bulk density for the hydrocarbon component, z_0 is the position of the first peak, B is the excess density of the first peak over bulk density, and λ is an exponential decay parameter for decrease in excess density over bulk from the first peak. This expression is an asymptotic form for the intrinsic density profile, and the parameters can

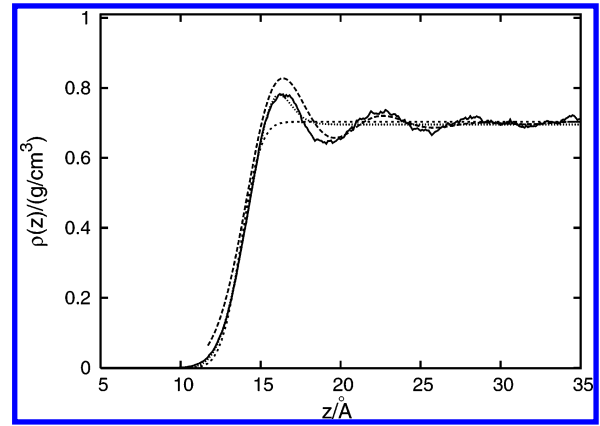


Figure 6. Density profiles $\rho(z)$ for TMP: obtained from simulation (solid line), obtained from the convolution of intrinsic density profile and distribution of surface positions (large dashes), fit to eq 6 (dots), and a fit to the error function profile (short dashes).

be obtained by fitting the height of the peaks in the intrinsic profile. As such, the functional form for the density profile obtained would be only approximate. Using eq 5, the Gaussian distribution of surface sites, and eq 1, one can obtain the following expression for the density profile

$$\rho(z) = \frac{A}{2} \left\{ 1 + \operatorname{erf} \left[\frac{z - z_1}{\sqrt{2}\sigma} \right] \right\} + \frac{B}{2} \exp \left(-\frac{z - z_2}{\lambda} \right) \left\{ 1 + \operatorname{erf} \left[\frac{z - z_3}{\sqrt{2}\sigma} \right] \right\} \quad (6)$$

where

$$z_2 = z_0 + \xi_0 + \frac{\sigma^2}{2\lambda} \quad \text{and} \quad z_3 = z_0 + \xi_0 + \frac{\sigma^2}{\lambda}$$

Density profiles from the simulation can be fit to this functional form and parameters compared with those obtained from simulation data. In Figure 6, we show the density profile obtained from simulation of the right side interface for TMP, the fit to eq 6, and a fit to an error function profile (eq 4). The first peak which is completely ignored in the error function profile is now better represented by eq 6 leading to a better model for the density profile. This improvement in fit is due to an increase in fit parameters, but there is a rationale for increasing the number of parameters. With a better representation of the intrinsic profile, a more accurate analytical expression for the density profile through the CA should be possible.

Instead of modeling the intrinsic profile and obtaining expressions for the density profile, one could start with the intrinsic density profile obtained in simulations and convolute it with the distribution of surface sites numerically. The density profile so obtained for TMP by convoluting⁵³ its intrinsic profile with respect to the water layer and the distribution of water surface positions is shown in Figure 6. The position of the first two peaks in the simulated density profile is accurately reproduced. The height of the first peak is somewhat overestimated while the height of the second peak obtained from the convolution is comparable with the simulated density profile. This validates the applicability of the CA for understanding density profiles. Clearly, including more details in the intrinsic profile model, beyond eq 5, is necessary for accurate representation of density profiles, and a simple error function profile can be misleading.

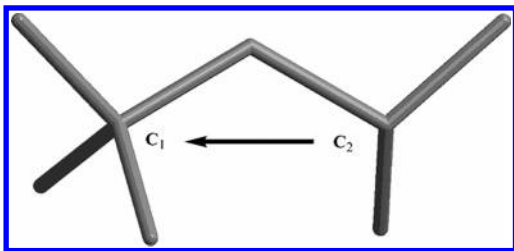


Figure 7. Vectors representing the hydrocarbon molecular orientation for TMP. The direction is from the less branched terminal nonmethyl site, C_2 , to the more branched terminal nonmethyl site, C_1 .

IV. Molecular Orientation

The orientation of molecules at and away from the interface can be studied by selecting a reference direction, a vector representing the molecular orientation and a suitably defined order parameter that quantifies molecular orientation with respect to the reference direction.

For the simulation setup selected here, the interface lies in the (x,y) plane and a natural reference direction is the unit normal to the interfacial plane, that is, the z -axis. With water being a planar molecule, its orientation in space can be uniquely determined in terms of the two O–H bond vectors. For hydrocarbon molecules, we identify the united atom sites (C_1 and C_2) to which the terminal methyl sites are attached. A unit vector is constructed between them in the direction from the less (C_2) to the more (C_1) bonded site and is shown pictorially for TMP in Figure 7.

With the reference direction and molecular orientation so defined, we quantify the orientation of molecule j in terms of the order parameter

$$S(\theta_j) = \frac{1}{2} \{3 \cos^2(\theta_j) - 1\} \quad (7)$$

where θ_j is the angle between the reference direction and a vector representative of molecule j 's orientation. The value of this order parameter is -0.5 for a molecule aligned perpendicular to the z -axis, 0 for isotropic orientation about the z -axis, and 1.0 for a molecule aligned parallel to the z -axis.

Instead of treating the two O–H covalent bonds as equivalent, we label the O–H vector with the smaller $S(\theta_j)$ type-A and the other bond is labeled type-B. Type-A O–H bonds therefore have an orientational bias toward being in the (x,y) plane and are likely to have negative order parameter values. Type-B O–H bonds on the other hand are biased toward the z -axis and are likely to have positive order parameter values.

Setting $X_j = S(\theta_j)$ in eq 3 and eq 2 and selecting the z -coordinate of the center of mass of molecule j as its position, we construct the orientation profile, $S(z)$, the intrinsic orientation profile $S_{L,Z}^{W-Y}(z)$, for water, and $S_I^{H-Y}(z)$, for the hydrocarbon, with respect to the surface formed by ($Y = H, W$) where Z is A or B for a type-A or type-B OH bond. To reduce noise in the results, data for each value of z is averaged over at least 10 molecules. The resulting intrinsic orientation profiles are presented in section IV A while the orientation profiles are presented in section IV B.

A. Intrinsic Orientation Profile. 1. Water. Intrinsic orientation profiles for each type of O–H bond can be constructed with respect to the surface water and hydrocarbon layers, for a total of four intrinsic profiles. These profiles should supplement our understanding of hydration structure near hydrophobic surfaces based on various density profiles. Just as for $\rho_1^{W-H}(z)$ and $\rho_1^{W-W}(z)$, there is weak dependence of $S_{L,\alpha}^{W-H}(z)$ and

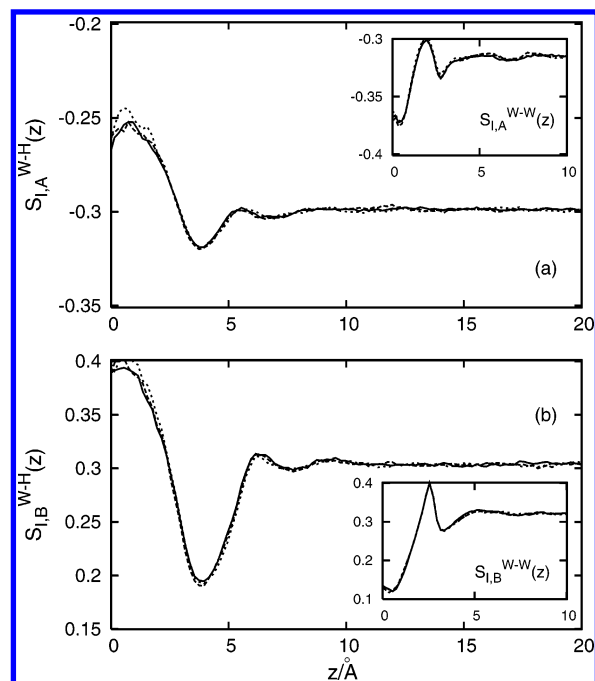


Figure 8. Intrinsic orientation profiles for (a) type-A O–H bond, $S_{L,A}^{W-H}(z)$, and (b) type-B O–H bonds, $S_{L,B}^{W-H}(z)$, of water with respect to the hydrocarbon surface in interfaces formed by P (solid line), 2MP (large dashes), and TMP (short dashes) (series 1). The shown inset is the corresponding profile with respect to the water surface.

$S_{L,\alpha}^{W-W}(z)$, where $\alpha = A, B$, on hydrocarbon branching. Intrinsic orientation profiles are therefore presented in Figure 8 for series 1 interfaces only.

The intrinsic orientation profiles, $S_{L,A}^{W-H}(z)$ and $S_{L,B}^{W-H}(z)$ reach asymptotic values of approximately -0.3 and ~ 0.3 , respectively. Far from the hydrocarbon surface, water should have bulklike isotropic orientation of these bonds. The order parameter value averaged over both type of O–H bonds is therefore zero asymptotically.

The first peak in $\rho_1^{W-H}(z)$ (Figure 2) at $z \sim 3.6$ Å arises due to a higher density of water molecules at this distance from the hydrocarbon surface. Corresponding to this position, there is a minimum in $S_{L,A}^{W-H}(z)$ implying a large bias of type-A O–H bonds toward orientation in the plane of the surface. For type-B O–H bonds, $S_{L,B}^{W-H}(z)$ shows a minimum at positive values indicating an orientational bias toward the surface normal. An increase in $S_{L,A}^{W-H}(z)$ is associated with an increase in $S_{L,B}^{W-H}(z)$. The orientation of the two O–H bonds for a water molecule are therefore not entirely independent. The minimum in the two profiles indicates an optimal alignment with the plane of the surface and is unaffected by the hydrocarbon component near it.

From the position of the first peak in $\rho_1^{W-H}(z)$, for $z \rightarrow 0$, the number of water molecules near the surface decreases. In this limit, the value of the two order parameters increases from the minimum. The type-A O–H bonds are less aligned with the plane of the surface while the type-B bonds tend to have a higher bias toward aligning perpendicular to the surface. The average O–H orientation has a value of ~ 0.15 which suggests molecules align with their O–H bonds pointing toward the hydrocarbon phase in its vicinity. On the other hand, $S_{L,A}^{W-H}(z)$ indicates a preferential alignment parallel to the surface. There are therefore two preferred orientations for molecules adjacent to the hydrocarbon surface in agreement with recent simulations by Jedlovsky and co-workers.^{54,55} The effect of hydrocarbon branch-

ing, although small, is to improve the alignment of an O—H bond with the surface normal closest to the hydrocarbon surface where differences in the branching should be most visible to molecules penetrating it.

Beyond the first peak for $z \rightarrow 20$ Å, $\rho_1^{W-H}(z)$ has a minimum at $z \sim 5.4$ followed by a second peak at $z \sim 7.2$ Å and a trough at $z \sim 8.4$ Å. The positions of the peaks correspond to local minima in $S_{1,\alpha}^{W-H}(z)$ for $\alpha = A, B$ whereas the positions of the troughs correspond to local maxima in the orientation profiles. There are therefore alternate regions of orientational bias toward the plane of the surface and toward the surface normal. Since peaks in $\rho_1^{W-H}(z)$ correspond to more molecules being at that position, it appears that more molecules align with the plane than with the surface normal at these separations from the surface. Of course, farther away, the net O—H order parameter value is zero implying an isotropic system.

Water structure beyond the surface layer in $\rho_1^{W-H}(z)$ is best studied with respect to the water surface as $\rho_1^{W-W}(z)$. The corresponding intrinsic orientation profiles for water, $S_{1,\alpha}^{W-W}(z)$ with $\alpha = A, B$, are shown in the inset of Figure 8 and do not reveal any effect of hydrocarbon branching. Molecules closest to the water surface layer are aligned with the surface. The average order parameter value for O—H bonds irrespective of their type is ~ 0.2 indicating a net ordering in the plane of the surface adjacent to the surface layer which in turn has a bias toward alignment with the surface normal. This arrangement is of course a consequence of hydrogen bonding.

Toward the first peak in $\rho_1^{W-W}(z)$ at $z \sim 2.6$ Å, the water molecules have one O—H bond preferably aligned with the surface normal leading to a peak in $S_{1,Z}^{W-W}(z)$, $Z = A, B$. The alternating behavior in orientation preference with respect to the water surface extends to the first peak. It should be noted that the peak in $S_{1,A}^{W-W}(z)$ is at $z \sim 2.2$ Å while the peak in $S_{1,B}^{W-W}(z)$ is shifted to $z \sim 2.5$ Å. The difference in position of these peaks implies the presence of two preferred orientations for O—H bonds at two distances from the water surface. This appears to be the reason behind the shoulder observed in the first peak of $\rho_1^{W-W}(z)$ (Figure 2b). Away from the water surface, the average O—H order parameter value tends to zero indicating an isotropic orientation in bulk.

2. Hydrocarbon. Analysis of surface molecules in section III A 2 suggested orientation of molecules along the surface. To probe this preference, the intrinsic orientation profile, $S_1^{H-W}(z)$, of hydrocarbon molecules with respect to the water surface is presented in Figure 9 for series 1 and 2.

The first peak in $\rho_1^{H-W}(z)$ at $z \sim 4$ Å has a corresponding minimum in $S_1^{H-W}(z)$. Molecules at this separation from the water surface have a strong bias toward orienting in the (x,y) plane and are the most likely contributors to p_a (Table 2). For series 1, hydrocarbon branching has no visible effect while series 2 hydrocarbons show an increase in magnitude of the order parameter. This would suggest longer molecules preferentially orient parallel to the water surface at this separation from the surface.

For $z < 4$ Å, hydrocarbon molecules penetrate the water surface. For series 1 hydrocarbons, there is a tendency toward isotropic orientation near the water layer. Perhaps due to comparable lengths, molecules in this series exhibit similar orientational preference in this region although isotropy of orientation follows the extent of bonding in the molecule. Series 2 hydrocarbon molecules that penetrate the water surface show a bias toward orienting in the interfacial plane unlike series 1 hydrocarbons which are more isotropic.

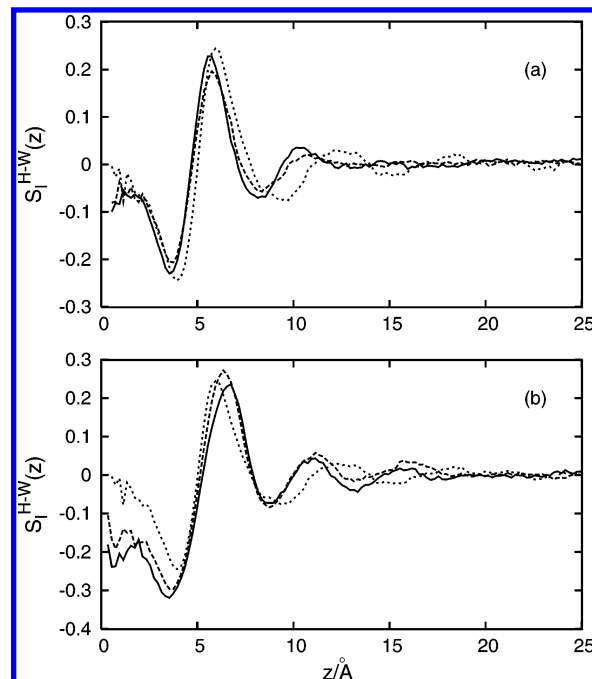


Figure 9. Intrinsic orientation profile of hydrocarbon molecules with respect to the water surface layer for (a) series 1: P (solid line), 2MP (large dashes), and TMP (small dashes); (b) series 2: O (solid line), 2MH (large dashes), and TMP (short dashes).

Beyond the first peak at $z \sim 4$ Å, there is a trough at ~ 6.2 Å followed by a second peak near $z \sim 10$ Å and a trough near $z \sim 13$ in $\rho_1^{H-W}(z)$. For each peak in the intrinsic density profile, there is a corresponding minimum in $S_1^{H-W}(z)$ and each trough in the intrinsic density profile has a corresponding peak in the orientation profile. It would appear that molecular orientational bias alternates from in-plane to perpendicular to the surface away from the water surface beyond the first peak. The magnitude of fluctuations between minima and ensuing maxima decreases away from surface until the system becomes isotropic. Hydrocarbon branching does not seem to have a significant impact on these intrinsic orientation profiles beyond the first peak except for the position of the peaks which shifts in tandem with the corresponding intrinsic density profile.

B. Orientation Profile. The effect of capillary wave broadening of intrinsic orientation profiles is illustrated here for type-A O—H bonds of water and the hydrocarbon C_1 — C_2 vector. Orientation profiles, $S(z)$, are constructed for these vectors and shown in Figure 10.

For type-A O—H bonds, $S_{1,A}^{W-H}(z)$ is shown in Figure 10a, and it reaches a bulk like value of -0.3 consistent with the corresponding intrinsic profile. Deviations from this asymptotic value are confined to the region $10 < z < 20$ Å with the number of molecules decreasing beyond $z = 15$ Å. The peak at $z \sim 15$ indicates a preferential alignment of one O—H bond parallel to the z -axis just as in $S_{1,A}^{W-H}(z)$. Deeper into the hydrocarbon phase, while $S_{1,A}^{W-H}(z)$ revealed a slight preference for aligning O—H bonds parallel to the surface, this information is not apparent in $S(z)$ and is perhaps lost in the noise.

The hydrocarbon orientation profile, $S(z)$, in Figure 10b, can be interpreted as $S_1^{H-W}(z)$ broadened by water surface fluctuations. The overall form of both profiles is similar. The first minimum in the intrinsic profile is broadened, but its magnitude in $S(z)$ at the minimum is comparable and implies orientation of hydrocarbon molecules parallel to the surface. While the intrinsic profile revealed a sharp increase from a minimum to

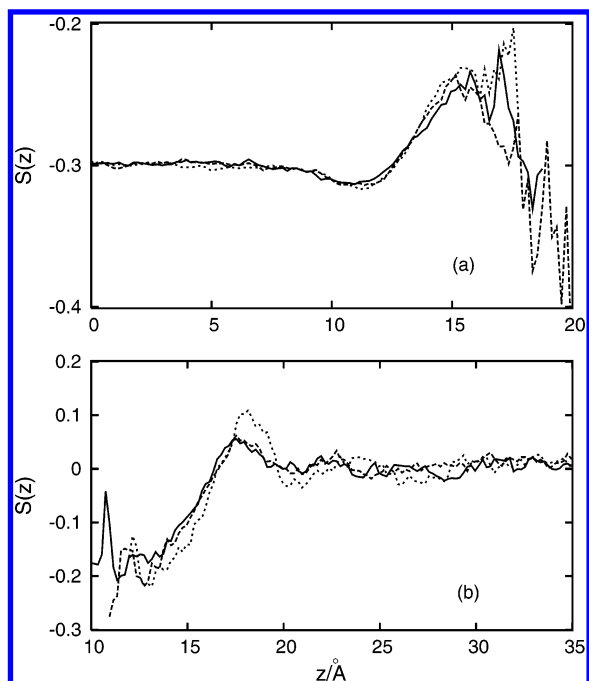


Figure 10. Orientation profile of (a) type-A O–H bonds and (b) hydrocarbon terminal C₁–C₂ vectors for hydrocarbon molecules in series 1: P (solid line), 2MP (large dashes), and TMP (small dashes).

a maximum, this too has been broadened in $S(z)$ due to surface fluctuations.

V. Hydrogen Bonding

The hydrogen bonded network structure of water is expected to be perturbed in the vicinity of an interface. An analysis of this network should complement the orientation information presented earlier. For this purpose, two water molecules are considered hydrogen bonded if their oxygen atoms are within 3.5 Å of each other and the angle made by the intermolecular O–O vector with the intramolecular O–H vector, for at least one O–H bond, is less than 30°. ⁵⁶

On the basis of this criterion, the network structure can be quantified in terms of the number of hydrogen bonds, N_j^{HB} , made with molecule j . Only molecules in the first coordination shell of molecule j (O–O distance less than 3.5 Å) can possibly form hydrogen bonds with it and they are enumerated. The percentage of first coordination shell molecules that form hydrogen bonds with molecule j , P_j^{HB} is another frequently calculated feature of the hydrogen bonded network. ⁵⁷

By defining $\mathbf{X}_j = N_j^{\text{HB}}$ and $\mathbf{X}_j = P_j^{\text{HB}}$ in eq 2 and eq 3, average profiles and intrinsic profiles for these quantities can be constructed. Parts a and b of Figure 11 show the intrinsic profiles, $N_1^{\text{HB}}(z)$ and $P_1^{\text{HB}}(z)$, with respect to the hydrocarbon surface. The shown inset is the usual $N^{\text{HB}}(z)$ and $P^{\text{HB}}(z)$ profile for the right water surface for series 1 interfaces. Series 2 interfaces are similar and not shown.

The intrinsic density profile for water, $\rho_1^{\text{w-H}}(z)$, shows a peak at $z \sim 3.6$ Å, a minimum at $z \sim 5.2$ Å, and the second peak at $z \sim 7.2$ Å. Molecules constituting the first peak show strong orientational bias toward aligning in the interfacial plane. The number of hydrogen bonds for these molecules however shows no unique features. Between the first and second peaks, orientational bias shifts from perpendicular to parallel and back to perpendicular to the surface normal. In this region, the number of hydrogen bonds increases monotonically from ~ 3.2 to ~ 3.9 , that is, toward bulklike values.

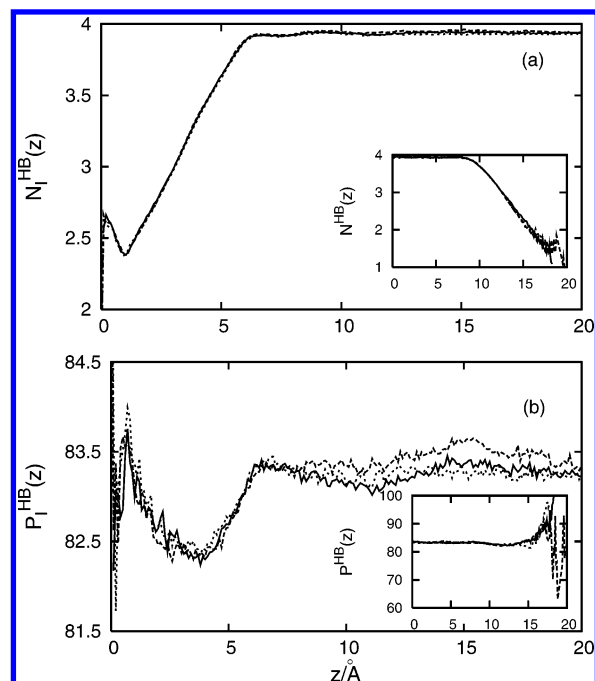


Figure 11. Intrinsic profiles for the two hydrogen network quantifiers (a) the number of hydrogen bonds, $N_1^{\text{HB}}(z)$, and (b) the percentage of first coordination shell molecules hydrogen bonded to a given water molecule, $P_1^{\text{HB}}(z)$, with respect to the hydrocarbon surface. Data are presented for series 1 hydrocarbons: P (solid lines), 2MP (large dashes), and TMP (small dashes). The shown insets in (a) and (b) are the corresponding profiles, $N^{\text{HB}}(z)$ and $P^{\text{HB}}(z)$, for water in system coordinates.

Closer to the hydrocarbon surface, water molecules preferentially align their O–H bonds toward the hydrophobic phase which reduces the number of hydrogen atoms available for hydrogen bond formation. There is a corresponding decrease in the number of hydrogen bonds formed from 3.2 at $z \sim 3.6$ Å to 2.4 at $z \sim 1$ Å. A larger fraction of molecules appears to form only two O···H bonds perhaps implying that two covalent O–H bonds face the hydrocarbon phase. For $0 < z < 1.0$ Å, the number of hydrogen bonds increases slightly to 2.7. This region corresponds to molecules biased toward orienting one O–H bond parallel to the surface thereby allowing for up to three hydrogen bonds. Branching on the hydrocarbon has a minimal effect on $N_1^{\text{HB}}(z)$ for both series 1 and 2 hydrocarbons.

The number of molecules available for hydrogen bonding changes at and away from the hydrocarbon surface. The position of the first peak in $\rho_1^{\text{w-H}}(z)$ corresponds to a region of enhanced density of oxygen sites. More molecules are available for hydrogen bonding in this region, and this leads to a minimum in $P_1^{\text{HB}}(z)$. Molecules at this separation from the hydrocarbon surface have one O–H bond aligned parallel to the surface and have a high coordination of 3. For $z \rightarrow 0$ from the first peak, $P_1^{\text{HB}}(z)$ increases up to a maximum at $z \sim 1$ Å. The number of water molecules available for hydrogen bonding must also decrease to account for this increase. For water molecules penetrating the hydrocarbon phase, $z < 1$ Å, one O–H bond is aligned parallel to the surface normal. The slight increase in $P_1^{\text{HB}}(z)$ corresponds to a higher percentage of water molecules being hydrogen bonded even though their number is smaller in this region.

The usual $N^{\text{HB}}(z)$ and $P^{\text{HB}}(z)$ profiles are presented in Figure 11 (insets) and arise from the smearing out of the intrinsic hydrogen bonded structure. The large z asymptotic value for $N^{\text{HB}}(z)$ and $N_1^{\text{HB}}(z)$ and $P^{\text{HB}}(z)$ and $P_1^{\text{HB}}(z)$ are equal and

represent bulk values. Fluctuation of the hydrocarbon surface broadens the small z structure visible in the intrinsic profile in addition to broadening the spatial region in which bulk to surface-like hydrogen bonding characteristics appear. The overall structure is in agreement with other simulations of water/hydrocarbon interfaces.^{29,31}

VI. Summary and Conclusions

Molecular dynamics simulations were performed for two series of hydrocarbons to gain insight into the effect of hydrocarbon branching on interfacial structure. For series 1, the chain length is fixed, whereas for series 2, molecular mass is kept fixed. Interfacial structure is broadened by capillary waves. We therefore identify a set of surface sites and construct intrinsic profiles with respect to them in the spirit of the CA.

For water, enhanced density near the hydrocarbon surface is primarily due to an increase in surface area over a planar surface. Density variations with respect to bulk values are confined to within 10 Å of the hydrocarbon surface. Hydrocarbon branching appears to have no discernible effect on intrinsic profiles of water. For the hydrocarbon phase, molecular orientation in the interfacial plane leads to enhanced density near the water surface. Series 1 hydrocarbon molecules have similar lengths, but the number of methyl sites increases with branching and is reflected in changes in intrinsic structure. For series 2, molecular length increases with a decrease in branching. Molecular orientation along the local surface is reduced primarily due to the geometric constraint of fitting molecules in the plane of the interface.

Molecular orientation with respect to the surface normal was quantified using an order parameter. For water, two distinct orientational preferences were identified. Molecules penetrating the hydrocarbon phase preferably orient one O–H bond toward it. Away from the hydrocarbon phase, molecular orientation switches from along the surface to along the surface normal and is associated with positive and negative deviations from bulk density. Hydrocarbon molecules tend to orient along the local surface adjacent to the water surface. For molecules that penetrate the water layer, orientational bias shifts from isotropic to perpendicular to the surface normal with decrease in branching, although series 2 hydrocarbons show a larger variation. Isotropic hydrocarbon orientation is observed beyond 22 Å from the water surface suggesting a minimum simulation box size for the hydrocarbon phase.

The hydrogen bonded network is perturbed near the interface with the number of hydrogen bonds per molecule decreasing monotonically from bulklike values toward the hydrocarbon surface. The number of molecules available for hydrogen bonding on the other hand decreases toward the hydrocarbon surface leading to a higher percentage of hydrogen bonded molecules. Molecules penetrating the hydrocarbon phase align one O–H bond with the surface normal toward the hydrocarbon phase and form up to three bonds efficiently. The number of hydrogen bonds for nonpenetrant surface water molecules shows the possible existence of water molecules with two H-bonds. Deviations from bulk are minimal and restricted to within 10 Å of the hydrocarbon surface in agreement with orientational information.

Hydrocarbon branching has an insignificant effect on water structure as observed in different intrinsic profiles. This insensitivity is perhaps an indication of the ability of water molecules to accommodate voids at the surface such that perturbation of the hydrogen bonded network is limited to a 10 Å region next to the hydrocarbon phase for all intrinsic profiles

studied here. The effect of branching on dynamics or the effect of the thermodynamic state on interfacial structure could be more significant and warrants further investigation. Branching, within the two series studied here, has a significant affect on all hydrocarbon intrinsic profiles.

A breakdown of the convolution approximation was observed by Chacon and Tarazona⁴⁵ for their atomic system due to correlations between surface positions and the intrinsic profiles. The convolution approximation was tested numerically based on the intrinsic density profiles and distribution of surface sites. Agreement between observed density profiles and convoluted intrinsic profiles was satisfactory perhaps due to implicit inclusion of correlations in our intrinsic profile construction. Structure in the intrinsic profiles is lost due to interface broadening by capillary waves and underlines their importance to studies of interfacial systems.

Acknowledgment. This work was supported by the Department of Energy Grant No. DE-FG03-0ZER15376.

References and Notes

- (1) Kazarinov, V. E. *The Interface Structure and Electrochemical Processes at the Boundary between Two Immiscible Liquids*; Springer: Berlin, 1987.
- (2) Gelbart, W. M.; Ben-Shaul, A.; Roux, D., Eds. *Micelles, membranes, microemulsions, and monolayers*; Springer-Verlag: New York, 1994.
- (3) Morrow, N. *Interfacial Phenomena in Petroleum Recovery*; Dekker: New York, 1990.
- (4) Southall, N. T.; Dill, K. A.; Haymet, A. D. J. *J. Phys. Chem. B* **2002**, *106*, 521.
- (5) Pratt, L. R.; Pohorille, A. *Chem. Rev.* **2002**, *102*, 2671.
- (6) Chandler, D. *Nature* **2005**, *437*, 640.
- (7) Benjamin, I. *Annu. Rev. Phys. Chem.* **1997**, *48*, 407.
- (8) Rowlinson, J. S.; Widom, B. *Molecular Theory of Capillarity*; Clarendon Press: Oxford, U.K., 1982.
- (9) van der Waals, J. *Verh. - K. Akad. Wet.* **1893**, *1*, 56. Rowlinson, J. *J. Stat. Phys.* **1979**, *20*, 97.
- (10) Cahn, J.; Hillard, J. *J. Chem. Phys.* **1958**, *28*, 258.
- (11) Fisk, S.; Widom, B. *J. Chem. Phys.* **1969**, *50*, 3219.
- (12) Buff, F.; Lovett, R.; Stillinger, F. *Phys. Rev. Lett.* **1965**, *15*, 621.
- (13) Weeks, J. D. *J. Chem. Phys.* **1977**, *67*, 3106.
- (14) Percus, J. R. In *Fluid Interfacial Phenomena*; Croxton, C. A., Ed.; John Wiley: New York, 1986; pp 1–44.
- (15) Sinha, S. K.; Sirota, E. B.; Garoff, S.; Stanley, H. B. *Phys. Rev. B* **1988**, *38*, 2297.
- (16) Mitrinovic, D. M.; Zhang, Z.; Williams, S. M.; Huang, Z.; Schlossman, M. L. *J. Phys. Chem. B* **1999**, *103*, 1779.
- (17) Mitrinovic, D. M.; Tikhonov, A. M.; Li, M.; Huang, Z.; Schlossman, M. L. *Phys. Rev. Lett.* **2000**, *85*, 582.
- (18) Sferrazza, M.; Xiao, C.; Jones, R. A. L.; Bucknall, D. G.; Webster, J.; Penfold, J. *Phys. Rev. Lett.* **1997**, *78*, 3693.
- (19) Rao, Y.; Comstock, M.; Eienthal, K. B. *J. Phys. Chem. B* **2006**, *110*, 1727.
- (20) Brown, M. G.; Walker, D. S.; Raymond, E. A.; Richmond, G. L. *J. Phys. Chem. B* **2003**, *107*, 237.
- (21) Rivera, J. L.; McCabe, C.; Cummings, P. T. *Phys. Rev. E* **2003**, *67*, 011603.
- (22) Carpenter, I. L.; Hehre, W. J. *J. Phys. Chem.* **1990**, *94*, 531.
- (23) Nicolas, J. P.; Smit, B. *Mol. Phys.* **2002**, *100*, 2471.
- (24) Nicolas, J. P.; de Souza, N. R. *J. Chem. Phys.* **2003**, *120*, 2464.
- (25) Wang, H.; Carlson, E.; Henderson, D.; Rowley, R. *Mol. Simul.* **2003**, *29*, 777.
- (26) Zhang, Y.; Feller, S. E.; Brooks, B. R.; Pastor, R. W. *J. Chem. Phys.* **1995**, *103*, 10252.
- (27) Patel, H. A.; Nauman, E. B.; Garde, S. *J. Chem. Phys.* **2003**, *119*, 9199.
- (28) Jedlovsky, P.; Varga, I.; Gilanyi, T. *J. Chem. Phys.* **2003**, *119*, 1731.
- (29) Michael, D.; Benjamin, I. *J. Phys. Chem.* **1995**, *99*, 1530.
- (30) van Buuren, A. R.; Marrink, S.-J.; Berendsen, H. J. C. *J. Phys. Chem.* **1993**, *97*, 9206.
- (31) Natalia, M.; Cordeiro, D. S. *Mol. Simul.* **2003**, *29*, 817.
- (32) Andersen, H. C. *J. Comput. Phys.* **1983**, *52*, 24.
- (33) Berendsen, H. J. C.; Grigera, J. R.; Straatsma, T. P. *J. Phys. Chem.* **1987**, *91*, 6269.

- (34) Jorgensen, W. L.; Madura, J. D.; Swenson, C. J. *J. Am. Chem. Soc.* **1984**, *106*, 6638.
- (35) Allen, W.; Rowley, R. L. *J. Chem. Phys.* **1997**, *106*, 10273.
- (36) Allen, M. P.; Tildesley, D. J. *Computer simulation of liquids*; Oxford University Press: Oxford, U.K., 1989.
- (37) Wolf, D.; Koblinski, P.; Phillpot, S. R.; Eggebrecht, J. *J. Chem. Phys.* **1999**, *110*, 8254.
- (38) Demontis, P.; Spanu, S.; Suffritti, G. B. *J. Chem. Phys.* **2001**, *114*, 7980.
- (39) Zahn, D.; Schilling, B.; Kast, S. M. *J. Phys. Chem. B* **2002**, *106*, 10725.
- (40) Sepiarsky, M.; Stachiotti, M. G.; Migoni, R. L. *Phys. Rev. B* **2005**, *72*, 014110.
- (41) Powles, J. G.; Rickayzen, G.; Heyes, D. M. *Mol. Phys.* **2005**, *103*, 1361.
- (42) Berendsen, H. J. C.; Postma, J. P. M.; van Gunsteren, W. F.; DiNola, A.; Haak, J. R. *J. Chem. Phys.* **1984**, *81*, 3684.
- (43) Frenkel, D.; Smit, B. *Understanding Molecular Simulations: From Algorithms to Applications*; Academic Press: San Diego, CA, 2002.
- (44) Chacon, E.; Tarazona, P. *Phys. Rev. Lett.* **2003**, *91*, 166103.
- (45) Tarazona, P.; Chacon, E. *Phys. Rev. B* **2004**, *70*, 235407.
- (46) Chacon, E.; Tarazona, P. *J. Phys.: Condens. Matter* **2005**, *17*, S3493.
- (47) Fernandes, P. A.; Natalia, M.; Cordeiro, D. S.; Gomes, J. A. N. F. *J. Phys. Chem. B* **1999**, *103*, 8930.
- (48) Pandit, S. A.; Bostick, D.; Berkowitz, M. L. *J. Chem. Phys.* **2003**, *119*, 2199.
- (49) Chowdhary, J.; Ladanyi, B. M. Manuscript in preparation.
- (50) Lee, C. Y.; McCammon, J. A.; Rossky, P. J. *J. Chem. Phys.* **1984**, *80*, 4448.
- (51) Ashbaugh, H. S.; Pratt, L. R.; Paulaitis, M. E.; Clohery, J.; Beck, T. L. *J. Am. Chem. Soc.* **2005**, *127*, 2808.
- (52) Chowdhary, J.; Ladanyi, B. M. Unpublished results.
- (53) Press, W. H.; Teukolsky, S. A.; Vetterling, W. H.; Flannery, B. P. *Numerical Recipes in C: The Art of Scientific Computing*; Cambridge University Press: Cambridge, U.K., 1997.
- (54) Jedlovsky, P.; Vincze, A.; Horvai, G. *J. Mol. Liq.* **2004**, *109*, 99.
- (55) Jedlovsky, P.; Vincze, A.; Horvai, G. *Phys. Chem. Chem. Phys.* **2004**, *6*, 1874.
- (56) Luzar, A.; Chandler, D. *Phys. Rev. Lett.* **1996**, *76*, 928.
- (57) Benjamin, I. *J. Chem. Phys.* **1992**, *97*, 1432.